RSC Advances

PAPER

View Article Online
View Journal | View Issue

Check for updates

Cite this: *RSC Adv.*, 2017, **7**, 34783

A comparative study of inter- and intramolecular C–H aminations: mechanism and site selectivity†

Juping Wang,*[a] Kangcheng Zheng,[b] Binbin Lin[a] and Yuping Weng[a]

The mechanism and site selectivity of inter-and intramolecular C–H bond aminations have been studied using the M06L method. The similarities and differences between inter- and intramolecular aminations are discussed in detail, with an emphasis on the correlation between reaction pathway and site selectivity. Our calculations show that, for both inter- and intramolecular aminations, the triplet stepwise pathway is of H-atom transfer character, while the singlet concerted pathway is of hydride-transfer character. More importantly, for intermolecular C–H bond amination, the triplet stepwise pathway is favored over the singlet one. Conversely, in the intramolecular case, the singlet concerted pathway is dominant. This inverse preference for the singlet–triplet pathway for inter- and intramolecular aminations is an important contributing factor to their inverse site selectivity. The calculated benzylic-to-tertiary (B : T) C–H amination ratios for the inter- and intramolecular aminations are 13 : 1 and 1 : 17, respectively, which are in agreement with experimental results of 7 : 1 and 1 : 7. Specifically, intermolecular amination favors oxidation of the secondary benzylic C–H bond over the tertiary C–H bond, whereas the intramolecular case shows a preference for tertiary C–H amination. This inverse site selectivity can be mainly attributed to the fact that inter- and intramolecular aminations proceed according to the different state pathways mentioned previously, where the enthalpic and entropic contribution to free energy differ. In addition, there is a higher energy barrier for the cleavage of the C–H bond in the intermolecular amination than in the intramolecular case, due to a much larger negative entropy of activation for the former. These results provide some valuable information for the design and deconstruction of highly selective and highly efficient C–H amination systems.

Received 4th May 2017
Accepted 24th June 2017

DOI: 10.1039/c7ra05032a

rsc.li/rsc-advances

Open Access Article. Published on 11 July 2017. Downloaded on 2/7/2026 5:24:19 AM.
This article is licensed under a Creative Commons Attribution-NonCommercial 3.0 Unported Licence.

1. Introduction

Selective functionalization of aliphatic C–H bonds to obtain a desired product is an exceptional challenge in organic and organometallic chemistry due to their abundance yet lack of reactivity.[1–5] In one of the most important C–H functionalization methods, catalytic C–H amination reactions can lead to novel C–N bond formation,[6–10] and this approach is widely applied to the synthesis of natural products, bioactive compounds, and materials.[11–14] Atom-, time-, and cost-efficient opportunities have made the field of C–H amination an active area of research.[15–20] In general, C–H amination is principally divided into two types:[7] intra-[21–23] and intermolecular[24–26] aminations. Relative to the large number of catalysts available for intramolecular amination, only a few transition-metal complexes can be employed effectively to catalyze the corresponding intermolecular reaction.[27–29] One of the top catalysts for performing both intra- and intermolecular C–H amination is $Rh_2^{II,II}(esp)_2$ (esp = α,α,α′,α′-tetramethyl-1,3-benzenedipropanoate), which was developed and first synthesized by Du Bois and coworkers[30,31] and shows good selectivity in the presence of multiple reactive sites. It is interesting to note that competition experiments reported by Du Bois and coworkers show that $Rh_2^{II,II}(esp)_2$-catalyzed intra- and intermolecular C–H aminations exhibit an opposite site selectivity in some cases.[32,33] As seen in Scheme 1, in the benzylic-to-tertiary competitive reaction of intramolecular amination, tertiary alkyl C–H bond insertion is favored over secondary benzylic oxidation. However, contrary to expectations, an analogous intermolecular competition reaction shows a preference for benzylic C–H amination. Such an exactly inverse benzylic-to-tertiary site selectivity attracts a great deal of attention, and various approaches have been made experimentally to tune or switch benzylic-to-tertiary selectivity by changing the metal core (such as Ag, Ru, Fe, *etc.*) or ligand of catalyst, modifying the substrate, and altering the nitrogen source.[32,34] Even so, the

[a]*School of Pharmacy, Guangdong Pharmaceutical University, Guangzhou, 510006, P. R. China. E-mail: jupingwang@gdpu.edu.cn*

[b]*School of Chemistry and Chemical Engineering, Sun Yat-sen University, Guangzhou, 510275, P. R. China*

† Electronic supplementary information (ESI) available: Intramolecular C–H amination process (Fig. S1), important frontier orbital diagrams of Rh2-nitrene (Fig. S2), mechanisms of intramolecular C–H aminations (Fig. S3), optimized structures for intermolecular aminations (Fig. S4), surface plots of the spin density distribution (Fig. S5), NBO charges for inter- and intramolecular aminations (Table S1), and the Cartesian coordinates for the calculated structures (Table S2). See DOI: 10.1039/c7ra05032a

Open Access Article. Published on 11 July 2017. Downloaded on 2/7/2026 5:24:19 AM.
This article is licensed under a Creative Commons Attribution-NonCommercial 3.0 Unported Licence.

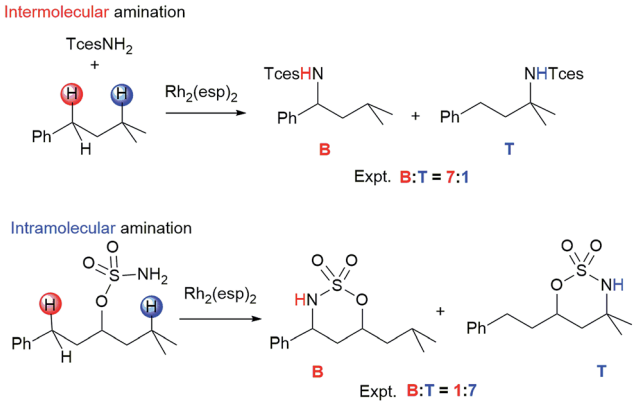

Scheme 1 Benzylic-to-tertiary site selectivity of inter- and intramolecular C–H aminations.

controlling factor for this site selectivity remains unresolved, and some newly designed amination systems fail to achieve the anticipation of high selectivity. We infer that the difference in site selectivity may be attributed to disparities in their complicated mechanisms. Therefore, efforts to improve catalyst and protocols for selective C–H amination are tied intimately to a thorough understanding of the mechanistic details of these reactions. Theoretical analyses based on density functional theory (DFT) calculations have become an essential tool to shed light on these mechanisms.[4a,13,35–37] To the best of our knowledge, to date, the site selectivity of dimetal-catalyzed C–H amination has been explored experimentally only, with no relative theoretical investigations. Over the past few years, we have performed some theoretical investigations on mechanisms of C–N/C–C bond formation by means of C–H functionalization,[38,39] and on the electronic structures and spectra of analogous transition-metal complexes.[40] Herein, in order to understand site-selective differences in nature between inter- and intramolecular C–H aminations and to further seek the defining factors of site selectivity, a DFT computational study was performed. Such an insight can also provide valuable information for designing and deconstructing catalytic inter- and intramolecular C–H amination systems of high selectivity and efficiency.

2. Computational details

DFT calculations were performed with the Gaussian 09 package,[41] using the M06L pure functional mode,[42] which has been found to be accurate for the energies and geometries of related C–H functionalization systems including multiple pathways.[37,38,43,44] In terms of the mechanism and selectivity of amination reactions, the steric effect is an important influencing factor, and sometimes even a governing factor.[3b,37,45] The catalyst $Rh_2^{II,II}(esp)_2$, involving two bulk esp ligands, would give rise to a considerable steric effect.[1,15,30] In order to obtain reliable computation results, we did not perform any simplification of the geometrical structures of any species in the reaction pathways. The geometries of all species were optimized in the gas phase at the basis set level below (denoted as BS1): the Stuttgart RSC 1997 Electron Core Potential (ECP) basis set with effective core potential and one additional f-type polarization function [ζ_f(Rh) = 1.350] was used for the Rh atom;[46] the 6-31G basis set[47] was used for the H, C, and O atoms in the $Rh_2^{II,II}(esp)_2$ unit of species; and a larger basis set 6-31G(d)[48] was used for the H, C, N, O, S, and Cl atoms in the nitrogen source and substrate moieties of species due to a more direct relevance to reactivity. For the optimized structures, the frequency calculations were also performed at the M06L/BS1 level in order to verify the energy minima (no imaginary frequencies) and transition states (one imaginary frequency). Intrinsic reaction coordinate (IRC)[49] calculations were carried out to determine the interconnection of the transition structures with the related reactants and products. Energies of the reported structures were improved by performing single-point energy calculations at the M06L level of theory with a larger basis set (denoted as BS2). The compositions of BS2 can be described as follows: the basis sets for the Rh atom and for the C, H, and O atoms in the $Rh_2^{II,II}(esp)_2$ unit were the same as those in BS1 but a higher-level basis set, 6-31G(d,p),[50] was used for C, H, O, S, and Cl atoms in the nitrogen source and substrate moieties of species. In order to estimate the effect of the solvent (toluene), a single-point energy calculation was performed at the M06L/BS2 level of theory, using Truhlar and coworkers' solvation model density (SMD) solvation model[51] on the gas-phase optimized geometries. All thermodynamic data discussed in the text are calculated at 298 K and 1 bar. Meanwhile, natural bond orbital (NBO) 6.0 analyses were performed at the M06L/BS2 level of theory.[52]

3. Results and discussion

Proposed catalytic cycles for intra- and intermolecular C–H aminations are shown in Fig. 1 and S1.† Clearly, the whole amination process can be divided into two parts: the formation of an $Rh_2^{II,II}$-nitrene intermediate and the insertion of an NR-group into the C–H bond. $Rh_2^{II,II}$-nitrene is considered a key catalytic intermediate and is directly responsible for the NR-group insertion into the C–H bond. It is worth pointing out that the competition of benzylic-to-tertiary C–H bond amination, as the focus in this context, begins with the same $Rh_2^{II,II}$-nitrene. For example, the intramolecular competitive amination starts from the nitrene of $Rh_2^{II,II}(esp)_2$-$NO_2SOC_{13}H_{19}$ and the intermolecular case begins in the nitrene of $Rh_2^{II,II}(esp)_2$-NTces. In other words, the site selectivity, whether for inter- or intramolecular C–H amination, depends solely on those reaction steps which follow the formed $Rh_2^{II,II}$-nitrene (*vide* the red box in Fig. 1 and S1†). Thus, our investigations on mechanism and site selectivity start from the $Rh_2^{II,II}$-nitrene.

In this work, the species involved in the reactions are listed as the $Rh_2^{II,II}(esp)_2$-nitrene intermediates (**X-^{n}IM1**), H-transfer transition states (**X-^{n}TS1$_Y$**), the radical intermediates (**X-^{3}IM2$_Y$**), C–N bond formation transition states (**X-^{3}TS2$_Y$**), and products (**X-^{1}PC$_Y$**), where X = A for intramolecular and R for intermolecular C–H aminations; n = 1 for singlet and 3 for triplet multiplicities; and Y = B for benzylic and T for tertiary C–H aminations. For the convenience of discussion, Scheme 2

This journal is © The Royal Society of Chemistry 2017

Open Access Article. Published on 11 July 2017. Downloaded on 2/7/2026 5:24:19 AM.
This article is licensed under a Creative Commons Attribution-NonCommercial 3.0 Unported Licence.

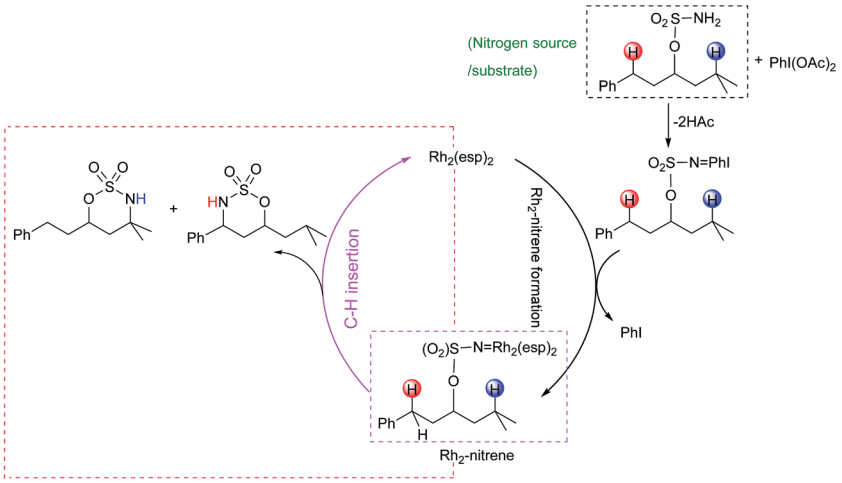

Fig. 1 Two parts of the intramolecular C–H amination process.

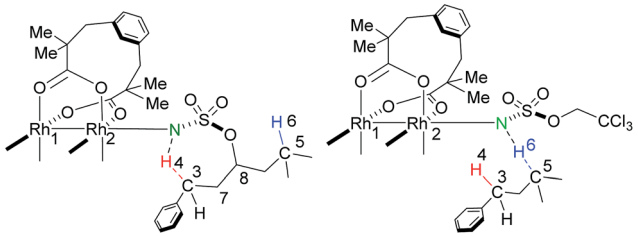

Scheme 2 Atom labels of all species in the intra- and intermolecular amination pathways.

presents labels of important atoms of species involved in the inter- and intramolecular C–H amination pathways.

3.1. Similarity of intra- and intermolecular aminations

As shown in Fig. 1 and S1,† for the intramolecular amination reaction, the $Rh_2^{II,II}$-nitrene **A-^{n}IM1** ($Rh_2^{II,II}(esp)_2$-$NO_2SOC_{13}H_{19}$) is composed of nitrenoid ($NO_2SOC_{13}H_{19}$) and $Rh_2^{II,II}(esp)_2$. In the subsequent C–H insertion process, the nitrenoid N-atom and reactive C–H bond come from the same nitrene intermediate. For the intermolecular amination reaction, the $Rh_2^{II,II}$-nitrene **R-^{n}IM1** ($Rh_2^{II,II}(esp)_2$-NTces) consists of nitrenoid (NTces) and $Rh_2^{II,II}(esp)_2$. In this case, the nitrenoid N-atom and reactive C–H bond come from the nitrene and substrate, respectively.

3.1.1. Reactivity of nitrene (A-^{n}IM1 and R-^{n}IM1). Investigation of the electronic structure and reactivity of $Rh_2^{II,II}$-nitrene can provide significant information for the amination reaction. Both **A-^{n}IM1** and **R-^{n}IM1** have two possible spin-state existences: singlet and triplet states (*i.e.* **A-^{1}IM1**/**R-^{1}IM1** and **A-^{3}IM1**/**R-^{3}IM1**). The orbital bonding patterns between the $Rh_2^{II,II}$ core and the N-atom are depicted in Fig. S2(a).† Important frontier orbitals and electron configurations for **A-^{n}IM1** and **R-^{n}IM1** are depicted in Fig. 2 and S2(b),† respectively. Among those orbitals shown in Fig. S2(a),† three-center (Rh–Rh–N) π* and σ* orbitals and $Rh_2^{II,II}$-centered δ* orbitals are very

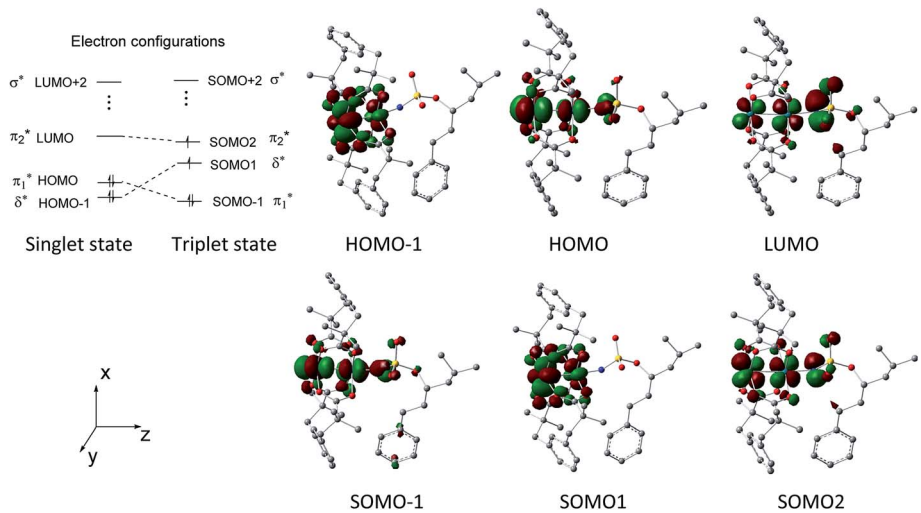

Fig. 2 Important Kohn–Sham frontier orbitals and electron configurations of A-^{1}IM and A-^{3}IM.

Open Access Article. Published on 11 July 2017. Downloaded on 2/7/2026 5:24:19 AM. This article is licensed under a Creative Commons Attribution-NonCommercial 3.0 Unported Licence.

important because they correspond to the calculated key frontier molecular orbitals (FMOs) of $Rh_2^{II,II}$-nitrene (highest occupied molecular orbital [HOMO]-1, HOMO and lowest unoccupied molecular orbital [LUMO] for singlet **A-^{1}IM1**; and SOMO1-1, SOMO1 and SOMO2 for triplet **A-^{3}IM1**) which would directly participate in the process of NR insertion into the C–H bond. Also, π* (π_1^* and π_2^*) and δ_2^* orbitals are close in energy. Similar energies allow the redistribution of one electron from the δ* to the π*, leading to differing population of the δ* and π* level in **A-^{1}IM1** and **A-^{3}IM1**. Thus, the configurations of the singlet **A-^{1}IM1** and triplet **A-^{3}IM1** are $(\delta^*)^2(\pi_1^*)^2(\pi_2^*)^0$ and $(\pi_1^*)^2(\delta^*)^1(\pi_2^*)^1$, respectively.

Fig. 2 shows that the HOMO-1, HOMO, LUMO of singlet **A-^{1}IM1** mainly consist of δ* (d_{xy})-Rh(d_{xy}), π_1^* Rh(d_{yz})-Rh(d_{yz})-N($sp^{2\prime\prime}$) and π_2^* Rh(d_{xz})-Rh(d_{xz})-N(p_x) antibonding orbitals, respectively. It is worth noting that the three-center (Rh–Rh–N) LUMO orbital has a significant N p contribution, which indicates that the LUMO of **A-^{1}IM1** can not only readily accept *two* electrons from the heterolytic cleavage of the σ_{C-H} bond through the N p_x orbital moiety but can also delocalize these electrons to the Rh_2 core *via* the Rh(d_{xz})–Rh(d_{xz}) moiety to increase the stability of the singlet transition state for hydride transfer. Thus, singlet **A-^{1}IM1** has a strongly *electrophilic* reactivity.

For triplet **A-^{3}IM1**, its singly occupied molecular orbital (SOMO)-1, SOMO1, SOMO2 orbitals are composed of π_1^* Rh(d_{yz})-Rh(d_{yz})-N(sp_y), δ* (d_{xy})-Rh(d_{xy}), and π_2^* Rh(d_{xz})-Rh(d_{xz})-N(p_x) antibonding orbitals, respectively. The three-center (Rh–Rh–N) SOMO2 orbital, in particular, has an obvious N p-character; moreover, its calculated unpaired spin densities are mainly located on the N-atom (0.984 e) and Rh_2 core (0.838 e) (see Fig. 5). This obvious N p-orbital character and almost a single electron on the N-atom indicates that the SOMO2 is readily accessible to accept *one* electron from the hemolytic cleavage of the σ_{C-H} bond. On the other hand, the Rh_2 core moiety of SOMO2 may bear considerable spins to avoid unpaired spins overly concentrating on the N-atom, facilitating crossing the triplet transition-state barrier for hydrogen-atom transfer. Therefore, triplet **A-^{3}IM1** has a high *radical* reactivity.

As shown in Fig. S2(b),† the orbital characters for intermolecular **R-^{1}IM1** and **R-^{3}IM1** are similar to intramolecular **A-^{1}IM1** and **A-^{3}IM1**, respectively, which indicates that, likewise, **R-^{1}IM1** also has strongly electrophilic reactivity and **R-^{3}IM1** has high radical reactivity.

Based on the above analysis, it can be concluded that both the singlet and triplet nitrenes can directly trigger NR insertion into the inert C–H bond. It should be noted that since the reactivity of nitrenes for intra- and intermolecular aminations is analogous, nitrene is not a defining factor contributing to inverse benzylic-to-tertiary site selectivity for intra- and intermolecular amination.

3.1.2. Mechanistic investigation of intra- and intermolecular aminations. It is assumed that there are singlet and triplet pathways for C–H amination reactions due to the existence of singlet and triplet nitrene.[7,37b,c,38] For intra- and intermolecular aminations, mechanistic details are depicted in Fig. 3 and S3,† and optimized geometries with important geometry parameters are depicted in Fig. 4 and S4,† respectively.

As depicted in Fig. 3 and S3,† for both intra- and intermolecular reactions, benzylic C–H amination mechanisms are analogous to tertiary ones. Herein, the benzylic C–H amination is given as an example to elaborate the characters of singlet and triplet pathways.

3.1.2.1. Character of singlet pathway. As mentioned above, LUMOs of singlet **A-^{1}IM1**/**R-^{1}IM1** accept two electrons from the heterolytic cleavage of σ_{C3-H4} to promote the singlet pathway. In the singlet pathway, **A-^{1}IM1**/**R-^{1}IM1** proceeds to the product **A-^{1}PC$_B$**/**R-^{1}PC$_B$** *via* the transition state **A-^{1}TS1$_B$**/**R-^{1}TS1$_B$**. The distances of C3···H4, N···H4, and C···N in **A-^{1}TS1$_B$**/**R-^{1}TS1$_B$** are 1.248/1.217 Å, 1.374/1.452 Å, and 2.586/2.661 Å, respectively, suggestive of a breaking C3···H4 bond and forming N···H4 and C···N bonds (see Fig. 3 and S3; and Fig. 4 and S4†). Moreover, in the subsequent ring-product **A-^{1}PC$_B$**/chain-product **R-^{1}PC$_B$**, the bond lengths of N–H4 and C3–N are 1.027/1.027 Å and 1.521/1.517 Å, respectively, indicating that both N–H4 and C3–N bonds are completely formed. All the above bond distances show that the formations of the N–H4 and C3–N bonds, as well as the cleavage of the C–H bond, proceed in a concerted manner. On the other hand, in the singlet pathway, there is a clear charge flow among reactive center N···H···C atoms: from **A-^{1}IM1**/**R-^{1}IM1+S** to **A-^{1}TS1$_B$**/**R-^{1}TS1$_B$**, the total NBO negative charges for the PhC moiety (*i.e.* Ph + C3) decrease greatly from −0.486/−0.494 to −0.268/−0.234 and negative charges for N-atom increase correspondingly from −0.690/−0.686 to −0.838/−0.870 (see Table 1). These change characteristics of NBO charges show that the H4 transferring process is accompanied by the partly negative charge of C3 flowing to the N-atom. Therefore, the singlet mechanisms of both intra- and intermolecular aminations are described as a concerted hydride-transfer pathway.

3.1.2.2. Character of triplet pathway. Unlike the singlet pathway, the triplet pathway begins in the triplet **A-^{3}IM1**/**R-^{3}IM.** The SOMO2 orbital of **A-^{3}IM1**/**R-^{3}IM** accepts *one* electron from the hemolytic cleavage of the σ_{C3-H4} bond to trigger triplet radical mechanism. Triplet pathway consists of two steps: H-abstract and radical rebound processes.

In the process of H-abstract, the H4 atom of the C3–H4 bond in **A-^{3}IM1**/**R-^{3}IM1** transfers to the metal-bound N-atom passing through the transition state **A-^{3}TS1$_B$**/**R-^{3}TS1$_B$.** As seen in Fig. 4 and S4,† the calculated **A-^{3}TS1$_B$**/**R-^{3}TS1$_B$** structure indicates an incipient N···H4 bond (1.330/1.368 Å) and an elongated C3···H4 bond (from 1.102/1.099 Å in **A-^{3}IM1+S**/**R-^{3}IM1** to 1.305/1.284 Å in **A-^{3}TS1$_B$**/**R-^{3}TS1$_B$**, respectively). Then, the C3–H4 bond breaks completely and an N–H4 bond forms completely to generate intermediate **A-^{3}IM2$_B$**/**R-^{3}IM2$_B$.** The surface plots and values of the spin density distribution of the triplet species for intra- and intermolecular benzylic C–H aminations are shown in Fig. 5 and S5,† respectively. The calculated spins show that **A-^{3}IM2$_B$**/**R-^{3}IM2$_B$** is a triplet radical species in which one unpaired electron is located on the Rh_2 core (0.676 e/0.734 e) and the other is located on C3 (0.800 e/0.768 e). In other words, the radical **A-^{3}IM2$_B$**/**R-^{3}IM2$_B$** formation is a result of the H-atom of

Open Access Article. Published on 11 July 2017. Downloaded on 2/7/2026 5:24:19 AM.
This article is licensed under a Creative Commons Attribution-NonCommercial 3.0 Unported Licence.

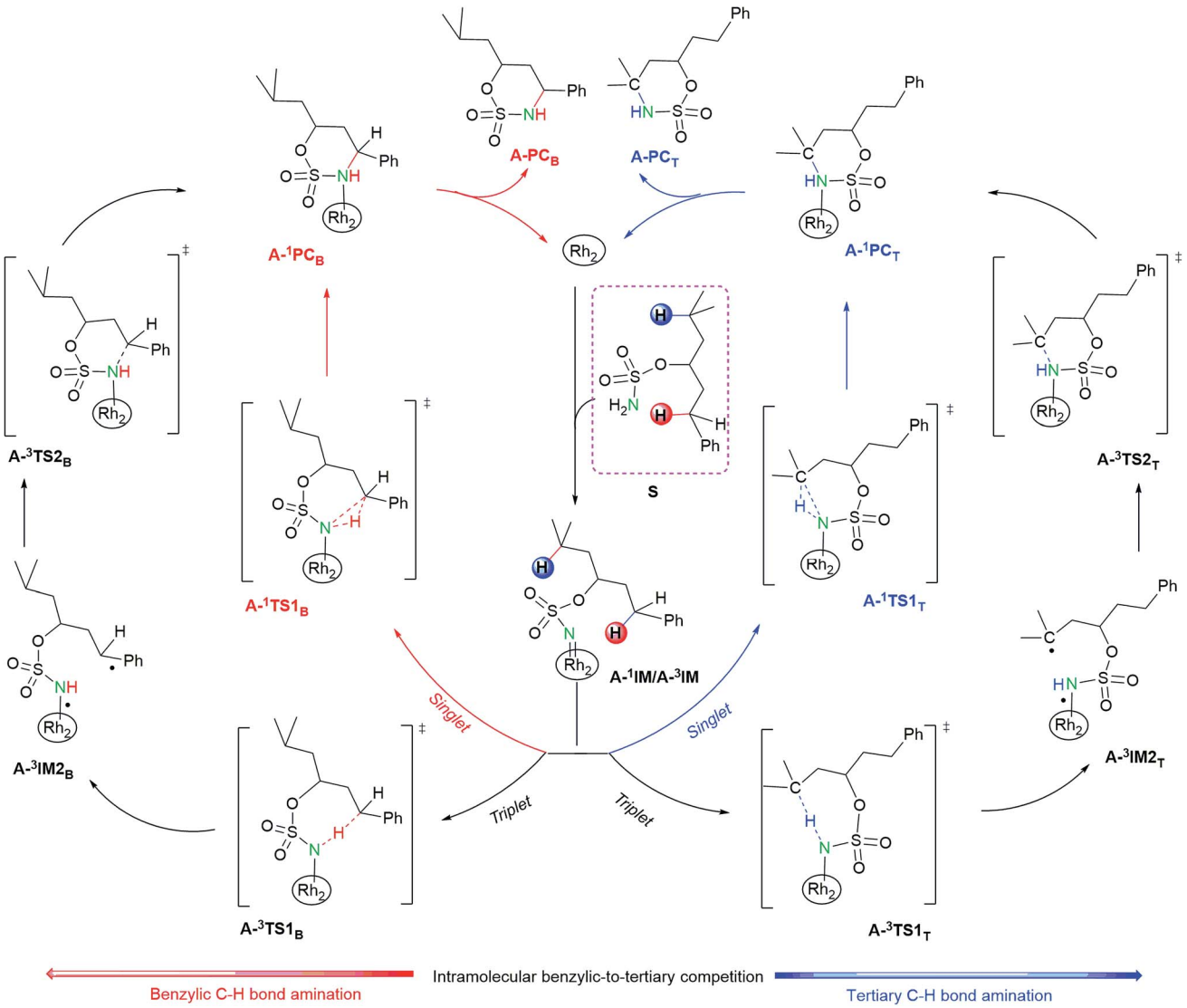

Fig. 3 Mechanisms of benzylic-to-tertiary C–H competition for intramolecular aminations. Herein, Rh_2 = $Rh_2(esp)_2$.

C3 transferring to the N-atom through the hemolytic cleavage of the σ_{C3-H4} bond.

In the subsequent C–N bond formation step, *via* the σ* orbital, the spin-transfer and inter-system crossing trigger the C3–N bond formation *via* the transition state **A-^{3}TS2$_B$**/**R-^{3}TS2$_B$** with an energy barrier of 5.6/11.4 kcal mol^{-1} (−2.4 → 3.2/−2.1 → 9.3 kcal mol^{-1}) (see Scheme 3). The whole processes for inter- and intramolecular benzylic C–H aminations are largely exergonic (−40.4 and −33.2 kcal mol^{-1}, respectively).

Based on the above discussions on the H-abstract and radical rebound processes, it can be concluded that the triplet mechanisms of both intra- and intermolecular aminations are characterized as a stepwise H-atom transfer pathway.

It should be noted that since the singlet and triplet pathways of intramolecular aminations are analogous to those of the respective intermolecular aminations, it may be difficult to cause inverse site selectivity if the intra- and intermolecular aminations simultaneously proceed as the singlet or triplet pathway. Their inverse site selectivity probably originated in different spin-state pathways (*vide* Section 3.2.).

3.2. Difference of inter- and intramolecular C–H aminations

Most interestingly, $Rh_2^{II,II}(esp)_2$, a robust tethered dicarboxylate-derived complex, shows good catalytic activity for both inter- and intramolecular C–H aminations, but with an inverse site selectivity. In this section, we will compare their mechanistic disparities in detail to gain a deeper understanding of this inverse selectivity. The enthalpy, entropy, and free energy of activation of all pathways for inter- and intramolecular aminations are listed in Table 2.

3.2.1. Comparison of free energy of activation. As shown in Table 2, all of the free energies of activation in the intermolecular hydrogen-transferring process ($\Delta G^{\neq}_{R,sol}$) are notably higher than those in the intramolecular process ($\Delta G^{\neq}_{A,sol}$) (14.0, 10.8, 12.7, and 11.9 kcal mol^{-1} > 5.5, 9.0, 3.4, and 6.5 kcal mol^{-1}). This can be explained by the difference between

Open Access Article. Published on 11 July 2017. Downloaded on 2/7/2026 5:24:19 AM.
This article is licensed under a Creative Commons Attribution-NonCommercial 3.0 Unported Licence.

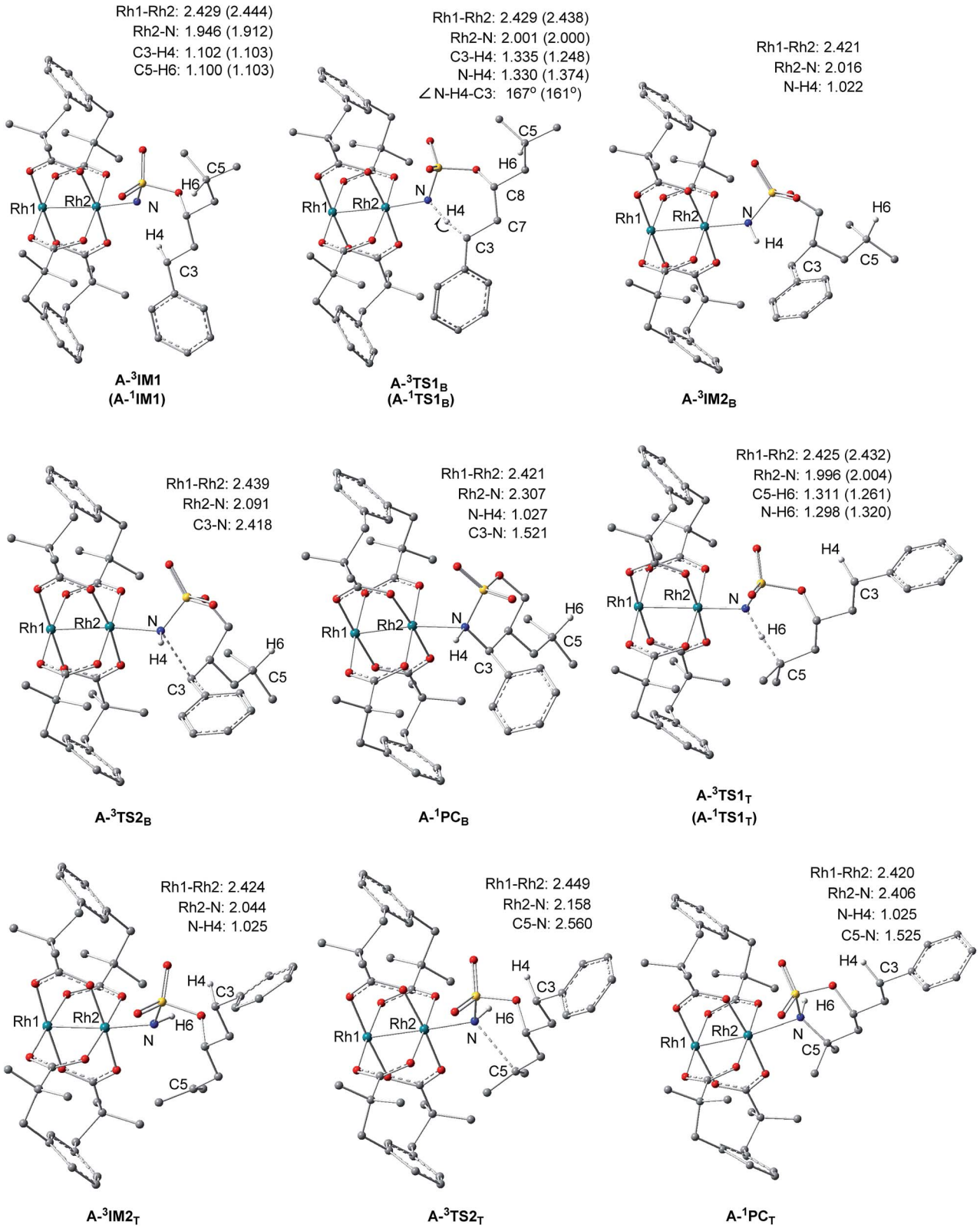

Fig. 4 Optimized structures and important geometrical parameters (bond lengths in Å, bond angles in degrees) of the species for intramolecular benzylic-to-tertiary C–H amination. Values without and with parentheses are for triplet and singlet states, respectively. For the sake of clarity, except for the reactive H4 and H6 atoms, all H-atoms are omitted.

This journal is © The Royal Society of Chemistry 2017

Open Access Article. Published on 11 July 2017. Downloaded on 2/7/2026 5:24:19 AM. This article is licensed under a Creative Commons Attribution-NonCommercial 3.0 Unported Licence.

Table 1 Calculated NBO charge (in e) for selected atoms in singlet pathways

Intramolecular amination			Intermolecular amination		
	C3 + Ph	N		C3 + Ph	N
A-^{1}IM1	−0.486	−0.690	**R-^{1}IM1+S**	−0.494	−0.686
A-^{1}TS1$_B$	−0.268	−0.838	**R-^{1}TS1$_B$**	−0.234	−0.870
A-^{1}PC$_B$	−0.065	−0.929	**R-^{1}PC$_B$**	−0.062	−0.924

enthalpic and entropic contributions to free energy. At constant temperature, the free energy of activation ($\Delta G^{\neq}$) can be divided into enthalpy ($\Delta H^{\neq}$) and entropy ($\Delta S^{\neq}$) of activation, by writing (eqn (1)):

$$\Delta G^{\neq} = \Delta H^{\neq} - T\Delta S^{\neq} \quad (1)$$

In terms of enthalpy aspects, all intermolecular $\Delta H^{\neq}_{R,sol}$ values are negative (−4.2, −4.4, −3.1, and −3.8 kcal mol^{-1}) whereas all intramolecular $\Delta H^{\neq}_{A,sol}$ values are positive (3.3, 6.6, 1.5, and 5.9 kcal mol^{-1}). Intermolecular $\Delta H^{\neq}_{R,sol}$ is beneficial to obtain a lower free energy of activation according to eqn (1), compared with $\Delta H^{\neq}_{A,sol}$. However, a larger difference comes from the entropy of activation; intermolecular $\Delta S^{\neq}_{R}$ values are −61.3, −50.9, −53.1, and −52.7 cal mol^{-1} K ($\Delta S^{\neq}_{R} \ll 0$) and intramolecular $\Delta S^{\neq}_{A}$ values are −7.3, −8.1, −6.1, and −1.9 cal mol^{-1} K^{-1} ($\Delta S^{\neq}_{A}$ is slightly less than zero). Obviously, all intermolecular $\Delta S^{\neq}_{R}$ values are much more negative, compared with intramolecular $\Delta S^{\neq}_{R}$ values. Indeed, the more negative intermolecular $\Delta S^{\neq}_{R}$ not only compensates for the influence of the enthalpy of activation previously described, but also further leads to a higher $\Delta G^{\neq}_{R,sol}$ *vs.* $\Delta G^{\neq}_{A,sol}$. The reason for a much more negative $\Delta S^{\neq}_{R}$ *vs.* $\Delta S^{\neq}_{A}$ is that two reactant species come together to form one species as intermolecular **R-^{n}IM1+S** proceeds to **R-^{n}TS1$_Y$** (see Fig. S3†). Entropy is a measure of the molecular disorder of a system, and the decrease in the number of molecules indicates that the disorder of the system is significantly reduced, thus the entropy is decreased remarkably. In contrast, an acyclic single molecule converts into a cyclic single molecule without any change in the number of molecules as intramolecular **A-^{n}IM1** proceeds to **A-^{n}TS1$_Y$** (see Fig. 3). This is also an entropy-decrease process, but the degree of entropy-decrease is much less compared with the intermolecular case. It is worth noting that the negative entropic contribution to **R-^{n}TS1$_Y$** is so significant that it has become the major thermodynamic factor controlling the free energy of activation. Hence, the intermolecular hydrogen-transferring process is predominantly entropy-driven, whereas the intramolecular process is both enthalpy- and entropy-driven combined. This difference will heavily impact the selectivities of the reaction pathway and the reaction site of inter- and intramolecular aminations (*vide* Sections 3.2.2. and 3.2.3.).

3.2.2. Comparison of preference of singlet–triplet pathway. Verifying the preference of different spin-state pathways of amination has become an active area of research due to a close connection with the selectivity and productivity of amination reactions.[4a,37a–c,53–56] Free energy profiles of inter- and intramolecular C–H amination are shown in Scheme 3, and for a clearer comparison, those values relevant to site selectivity are shown in Table 3.

As shown in Table 3 and Scheme 3, for intermolecular aminations, the calculated energy barrier of singlet **R-^{1}TS1$_B$**/**R-^{1}TS1$_T$** is higher than that of the corresponding triplet **R-^{3}TS1$_B$**/**R-^{3}TS1$_T$** (**R-^{1}TS1$_B$** *vs.* **R-^{3}TS1$_B$** = 14.0 *vs.* 10.8 kcal mol^{-1}; and **R-^{1}TS1$_T$** *vs.* **R-^{3}TS1$_T$** = 12.7 *vs.* 11.9 kcal mol^{-1}). Conversely, in the intermolecular case, the energy barrier of singlet **A-^{1}TS1$_B$**/**A-^{1}TS1$_T$** is significantly lower than that of the corresponding triplet **A-^{3}TS1$_B$**/**A-^{3}TS1$_T$** (**A-^{1}TS1$_B$** *vs.* **A-^{3}TS1$_B$** = 5.5 *vs.* 9.0 kcal mol^{-1}; and **A-^{1}TS1$_T$** *vs.* **A-^{3}TS1$_T$** = 3.4 *vs.* 6.5 kcal mol^{-1}). In other words, the triplet stepwise pathway is dominant for intermolecular benzylic and tertiary C–H aminations. In contrast, the singlet concerted pathway is favored over the triplet stepwise pathway for intramolecular benzylic and tertiary C–H aminations. The differences of preference in the singlet–triplet pathway between the inter- and intramolecular hydrogen-transferring processes can be explained by the drive mechanism mentioned previously. Herein, benzylic sites are given as an example to illustrate the reason for the preference of the singlet–triplet pathway.

In the intermolecular case, free energies of activation for singlet and triplet pathways are both entropy-driven, which is mainly related to the disorder of the system. However, the N, H, and C atoms of the reactive center have a trigonal arrangement ($_{N}\!<\!^{H}_{}\!>\!_{C}$) in singlet **R-^{1}TS1$_B$** and are almost linear (N···H···C) in triplet **R-^{3}TS1$_B$** (see Scheme. 3(a)). Clearly, the former has less

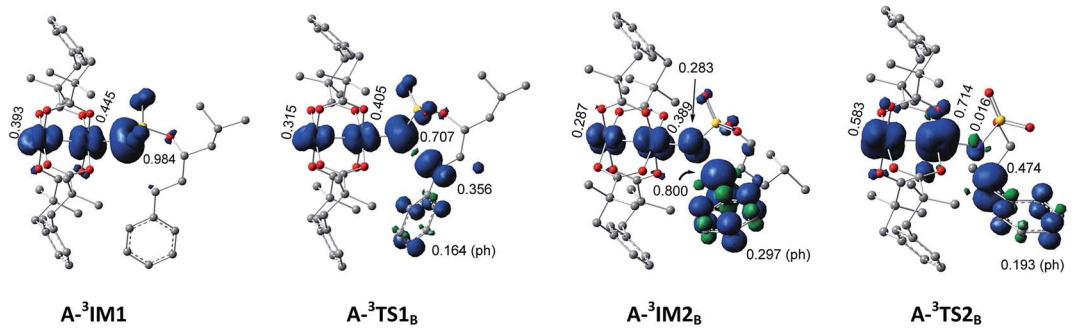

Fig. 5 Surface plots and values of spin density distribution of the triplet species for intramolecular benzylic C–H amination.

Open Access Article. Published on 11 July 2017. Downloaded on 2/7/2026 5:24:19 AM.
This article is licensed under a Creative Commons Attribution-NonCommercial 3.0 Unported Licence.

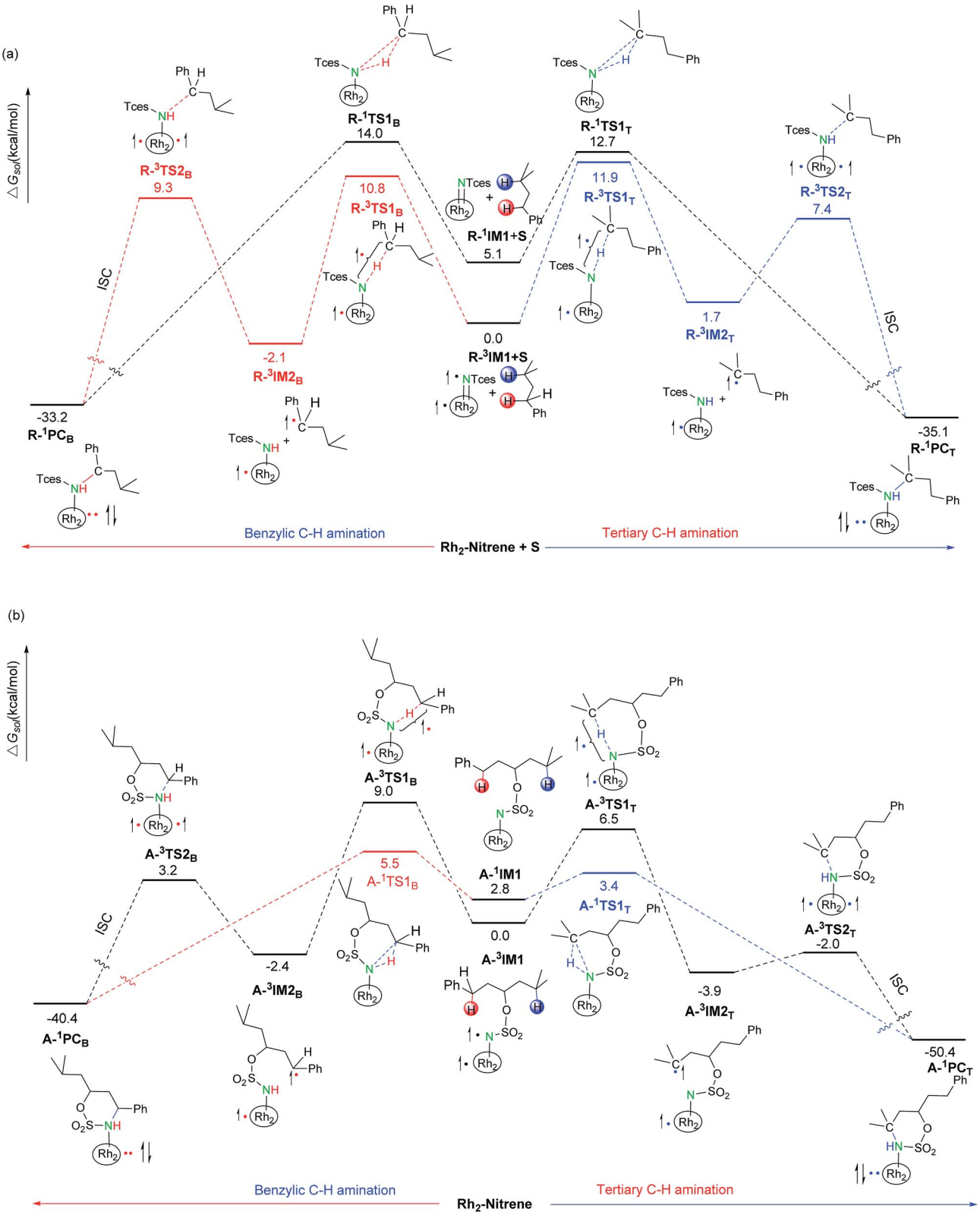

Scheme 3 (a) Free energy profiles of intermolecular C–H amination. (b) Free energy profiles of intramolecular C–H amination. Herein, · and 1 stand for the unpaired election and its spin direction, respectively.

This journal is © The Royal Society of Chemistry 2017

Open Access Article. Published on 11 July 2017. Downloaded on 2/7/2026 5:24:19 AM.
This article is licensed under a Creative Commons Attribution-NonCommercial 3.0 Unported Licence.

Table 2 Comparison of enthalpy (kcal mol^{-1}), entropy (cal mol^{-1} K^{-1}), and free energy (kcal mol^{-1}) of activation between inter- and intramolecular aminations

Intermolecular aminations				Intramolecular aminations			
	$\Delta H^{\neq}_{R,sol}$	$\Delta S^{\neq}_{R}$	$\Delta G^{\neq}_{R,sol}$		$\Delta H^{\neq}_{A,sol}$	$\Delta S^{\neq}_{A}$	$\Delta G^{\neq}_{A,sol}$
R-^{3}IM1+S	0.0	0.0	0.0	**A-^{3}IM1**	0.0	0.0	0.0
R-^{1}TS1$_B$	−4.2	−61.3	14.0	**A-^{1}TS1$_B$**	3.3	−7.3	5.5
R-^{3}TS1$_B$	−4.4	−50.9	10.8	**A-^{3}TS1$_B$**	6.6	−8.1	9.0
R-^{1}TS1$_T$	−3.1	−53.1	12.7	**A-^{1}TS1$_T$**	1.5	−6.1	3.4
R-^{3}TS1$_T$	−3.8	−52.7	11.9	**A-^{3}TS1$_T$**	5.9	−1.9	6.5

Table 3 Comparison of free energy of activation of inter- and intramolecular C–H aminations

	Intermolecular aminations				Intramolecular aminations		
	R-^{1}TS1$_Y$[a]	**R-^{3}TS1$_Y$**[a]	Pref.[b]		**A-^{1}TS1$_Y$**[a]	**A-^{3}TS1$_Y$**[a]	Pref.[b]
B	14.0	10.8	Triplet	B	5.5	9.0	Singlet
T	12.7	11.9	Triplet	T	3.4	6.5	Singlet
B : T	—	13 : 1^{Calcd} 7 : 1$^{Expt.}$	—	B : T	1 : 17^{Calcd} 1 : 7$^{Expt.}$	—	—

[a] Subscript Y stands for B or T. [b] Pref. represents a preferable pathway for the corresponding amination reaction.

disorder, and a larger negative entropy of activation (−61.3 *vs.* −50.9 cal mol^{-1} K^{-1}), which leads to a larger free energy of activation (14.0 *vs.* 10.8 kcal mol^{-1}). Therefore, the triplet stepwise pathway is preferable to the singlet concerted pathway in the intermolecular amination reaction.

In the intramolecular case, the difference of activation free energy of the singlet and triplet pathways predominantly arises from their activation enthalpies, which are closely related to bond cleavage and formation. In singlet **A-^{1}TS1$_B$**, the cleavage of a C–H bond is accompanied by the formation of two new bonds (N–H and C–N), while in triplet **A-^{3}TS1$_B$**, the cleavage of a C–H bond is only accompanied by the formation of one new bond (N–H). Bond formation and cleavage are exothermic and endothermic, respectively. Therefore, singlet $\Delta H^{\neq}_{A,sol}$ (**A-^{1}TS1$_B$**) is smaller than triplet $\Delta H^{\neq}_{A,sol}$ (**A-^{3}TS1$_B$**) (3.3 *vs.* 6.6 kcal mol^{-1}), which results in a lower $\Delta G^{\neq}_{A,sol}$ (**A-^{1}TS1$_B$**) compared with $\Delta G^{\neq}_{A,sol}$ (**A-^{3}TS1$_B$**) (5.5 *vs.* 9.0 kcal mol^{-1}). In other words, the singlet pathway is more favorable than the triplet pathway for the intramolecular hydrogen-transferring processes, which is precisely contrary to the intermolecular case.

It is worth noting that the inverse preferences of the singlet–triplet pathway for inter- and intramolecular C–H amination are an important contributing factor to their inverse site selectivity (*vide* Section 3.2.3.).

3.2.3. Comparison of site selectivity. Our computational studies above are consistent with a triplet pathway for intermolecular aminations and a singlet pathway for the intramolecular. Therefore, the product ratio of benzylic-to-tertiary (B : T) only depends on the activation free energies of intermolecular triplet **R-^{3}TS1$_Y$** and intramolecular singlet **A-^{1}TS1$_Y$**, since the benzylic site contains two equally reactive C–H bonds whereas the tertiary site contains only a single 3° C–H bond. Thus, the ratio of B : T can be calculated using eqn (2), where B and T represent the benzylic and tertiary products, respectively; and $\Delta G^{\neq}_{B}$ and $\Delta G^{\neq}_{T}$ represent the activation free energies of the benzylic and tertiary hydrogen-migrating step, respectively.

$$\frac{B}{T} = \frac{2k_B}{k_T} = \frac{2\exp\left(-\Delta G^{\neq}_{B}/RT\right)}{\exp\left(-\Delta G^{\neq}_{T}/RT\right)} \quad (2)$$

It can be seen from Table 3 that the energy barrier of **R-^{3}TS1$_B$** for the benzylic hydrogen-transfer is favored by 1.1 kcal mol^{-1} over **R-^{3}TS1$_T$** for the tertiary (11.9–10.8 = 1.1 kcal mol^{-1}), while the energy barrier of **A-^{1}TS1$_B$** for benzylic C–H amination is 2.1 kcal mol^{-1} higher than that of **A-^{1}TS1$_T$** for tertiary C–H amination (5.5–3.4 = 2.1 kcal mol^{-1}). Based on eqn (2), the calculated ratios of benzylic-to-tertiary (B : T) for inter- and intramolecular C–H aminations are 13 : 1 and 1 : 17, respectively, which is in accordance with the experimental results (7 : 1 and 1 : 7, respectively). In other words, intermolecular amination favors oxidation of benzylic C–H bonds over tertiary sites, while the intramolecular case exhibits a preference for tertiary C–H amination.

The selective amination of the secondary benzylic C–H bond over the tertiary alkyl C–H bond in the intermolecular case is closely related to their triplet stepwise pathways, in which the transition states **R-^{3}TS1$_B$** and **R-^{3}TS$_T$** are clearly of radical character. For **R-^{3}TS1$_B$**, two unpaired electrons are populated on the Ph group (0.198 e), and the C3 (0.357 e), N (0.641 e), and Rh_2 (0.712 e) atoms (see Fig. 6). For **R-^{3}TS1$_T$**, the unpaired spins mainly reside on the C5 (0.439 e), N (0.649 e), and Rh_2 (0.770 e) atoms. Quite remarkably, the unpaired electron has been greatly delocalized to the Ph group adjacent to the C3 atom by a p–π conjugation in **R-^{3}TS1$_B$**, which is absent in **R-^{3}TS1$_T$**. It is important to note that this wider delocalization of spins can increase the stability and reduce the enthalpy of **R-^{3}TS1$_B$**. Therefore, the activation enthalpy $\Delta H^{\neq}_{R,sol}$ (**R-^{3}TS1$_B$**) is lower than $\Delta H^{\neq}_{R,sol}$ (**R-^{3}TS1$_T$**) (−4.4 *vs.* −3.8 kcal mol^{-1}). On the other hand, the bulky Ph group and esp unit are far away from each other in **R-^{3}TS1$_B$** but close to each other in **R-^{3}TS1$_T$** (see Fig. 7), resulting in less steric hindrance, and a smaller negative

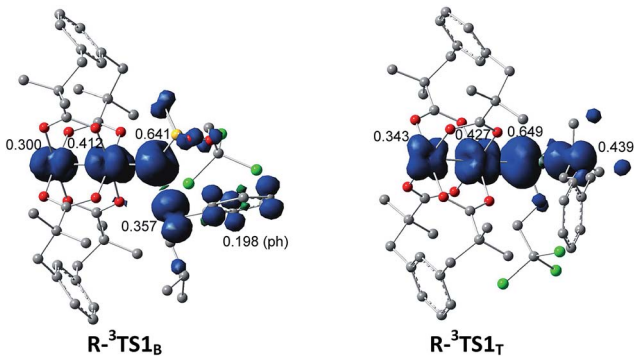

Fig. 6 Surface plots and values of spin density distribution for R-^{3}TS1$_B$ and R-^{3}TS1$_T$.

Open Access Article. Published on 11 July 2017. Downloaded on 2/7/2026 5:24:19 AM.
This article is licensed under a Creative Commons Attribution-NonCommercial 3.0 Unported Licence.

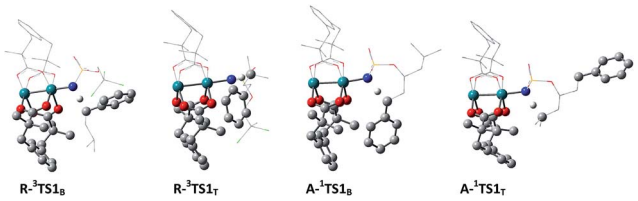

Fig. 7 Steric hindrance between phenyl (Ph) group and esp ligand. The other H atoms except reactive H are omitted for clarity.

entropy of activation for **R-^{3}TS1$_B$** *vs.* **R-^{3}TS1$_T$** (−50.9 *vs.* −52.7 kcal mol^{-1}). A lower enthalpy of activation and a smaller negative entropy of activation for **R-^{3}TS1$_B$** lead to the fact that the activation free energy of **R-^{3}TS1$_B$** is lower than that of **R-^{1}TS1$_B$**, thus a preference for the benzylic site in the intermolecular amination.

In contrast, the site selectivity toward tertiary C–H bond amination in the intramolecular case can be explained as follows. Intramolecular C–H amination is corroborated as a singlet concerted pathway in which the transition states **A-^{1}TS1$_T$** and **A-^{1}TS1$_B$** clearly show signs of the breaking of a C–H bond along with the forming of an N–H bond and a C–N bond. The N···H distance of 1.320 Å and C···N distance of 2.572 Å in **A-^{1}TS1$_T$** is shorter than that of 1.374 and 2.586 Å in **A-^{1}TS1$_B$**, respectively, which suggests that the formations of both N···H and C···N bonds are more complete in **A-^{1}TS1$_T$** than in **A-^{1}TS1$_B$**. Because bond formation is exothermic, the activation enthalpy for **A-^{1}TS1$_T$** is less than that for **A-^{1}TS1$_B$** (1.5 *vs.* 3.3 kcal mol^{-1}). Furthermore, the bulky Ph group and esp unit are far away from each other in **A-^{1}TS1$_T$** but close to each other in **A-^{1}TS1$_B$** (see Fig. 7), resulting in less steric hindrance, and a smaller negative entropy of activation for **A-^{1}TS1$_T$** *vs.* **A-^{1}TS1$_B$** (−6.1 *vs.* −7.3 kcal mol^{-1}). A lower enthalpy of activation and a smaller negative entropy of activation of **R-^{3}TS1$_B$** leads to the fact that the activation free energy $\Delta G^{\neq}_{A,sol}$ (**A-^{1}TS1$_T$**) is lower than $\Delta G^{\neq}_{A,sol}$ (**A-^{1}TS1$_B$**) (3.4 *vs.* 5.5), thus tertiary site C–H amination is more favorable than the benzylic site in the intramolecular case.

4. Conclusion

This paper presents a theoretical investigation of the mechanism and site selectivity of inter- and intramolecular aminations. The similarities and differences of inter- and intramolecular aminations are discussed in detail. Most importantly, we report that inter- and intramolecular C–H bond aminations proceed as different spin-state pathways, and this difference is an important factor contributing to their inverse benzylic-to-tertiary site selectivity. According to the computational results, the following main conclusions can be drawn:

(1) The reactivity of inter- and intramolecular $Rh_2^{II,II}$-nitrene intermediates are analogous. Singlet **A-^{1}IM1/R-^{1}IM1** has strongly electrophilic reactivity and triplet **A-^{3}IM1/R-^{3}IM1** has highly radical reactivity.

(2) For both inter- and intramolecular aminations, the singlet mechanism is described as a concerted hydride-transfer pathway, while the triplet mechanism is of stepwise H-atom transfer character.

(3) All of the free energies of activation in the intermolecular hydrogen-transferring process ($\Delta G^{\neq}_{R,sol}$) are clearly higher than those in the intramolecular process ($\Delta G^{\neq}_{A,sol}$). The intermolecular hydrogen-transferring process is mainly entropy-driven, whereas the intramolecular case is both enthalpy- and entropy-driven combined.

(4) For the intermolecular C–H amination, the triplet stepwise pathway is favored over the singlet process. Conversely, for the intramolecular C–H amination, the singlet concerted pathway is dominant. The inverse preferences of the singlet–triplet pathway for inter- and intramolecular C–H amination are an important factor contributing to their inverse site selectivity.

(5) Inter- and intramolecular C–H aminations display an inverse site selectivity with calculated B : T ratios of 13 : 1 and 1 : 17, respectively, which is in agreement with experimental results (7 : 1 and 1 : 7, respectively). The intermolecular insertion reaction shows a preference for the benzylic site as a result of a preferential triplet pathway, in which a lower enthalpy of activation and a smaller negative entropy of activation of **R-^{3}TS1$_B$** mean that the activation free energy of **R-^{3}TS1$_B$** is lower than that of **R-^{3}TS1$_T$**. That intramolecular tertiary C–H bond insertion is more favorable than the benzylic case can be attributed to a preferential singlet concerted pathway, in which a lower enthalpy of activation and a smaller negative entropy of activation of **A-^{1}TS1$_T$** mean that the activation free energy of **A-^{1}TS1$_T$** is lower than that of **A-^{1}TS1$_B$**.

This computational study has provided valuable information about inter- and intramolecular aminations, with an emphasis on addressing the correlation between reaction pathways and site selectivity. These conclusions can be applied to deconstruct the elegant and highly selective catalytic amination systems, especially the more challenging intermolecular C–H amination systems.

Acknowledgements

This work was financially supported by the Medical Scientific Research Foundation of Guangdong Province, China (no. A2015556), Special Program for Applied Research on Super Computation of the NSFC-Guangdong Joint Fund (the second phase), Natural Science Foundation of Guangdong Province, China (No. 2015A030310176), Natural Science Foundation for Young Scholars of College of Pharmacy of Guangdong Pharmaceutical University (2014), and Science and Technology Planning Project of Guangdong Province, China (no. 2013J4100071).

Notes and references

1 (*a*) J. L. Roizen, M. E. Harvey and J. Du Bois, *Acc. Chem. Res.*, 2012, **45**, 911–922; (*b*) H. M. L. Davies, J. Du Bois and J.-Q. Yu, *Chem. Soc. Rev.*, 2011, **40**, 1926–1936; (*c*) J. Du Bois, *Org. Process Res. Dev.*, 2011, **15**, 758–762.

2 (*a*) S. R. Chemler, *Science*, 2013, **341**, 624–626; (*b*) M. C. White, *Science*, 2012, **335**, 807–809.

 This journal is © The Royal Society of Chemistry 2017

Open Access Article. Published on 11 July 2017. Downloaded on 2/7/2026 5:24:19 AM.
This article is licensed under a Creative Commons Attribution-NonCommercial 3.0 Unported Licence.

3 (*a*) H. M. L. Davies and D. Morton, *J. Org. Chem.*, 2016, **81**, 343–350; (*b*) H. M. L. Davies and J. R. Manning, *Nature*, 2008, **451**, 417–424.
4 (*a*) M. Goswami, V. Lyaskovskyy, S. R. Domingos, W. J. Buma, S. Woutersen, O. Troeppner, I. Ivanović-Burmazović, H. Lu, X. Cui, X. P. Zhang, E. J. Reijerse, S. DeBeer, M. M. van Schooneveld, F. F. Pfaff, K. Ray and B. de Bruin, *J. Am. Chem. Soc.*, 2015, **137**, 5468–5479; (*b*) H. Lu, C. Li, H. Jiang, C. L. Lizardi and X. P. Zhang, *Angew. Chem.*, 2014, **126**, 7148–7152.
5 J. Yamaguchi, A. D. Yamaguchi and K. Itami, *Angew. Chem., Int. Ed.*, 2012, **51**, 8960–9009.
6 E. T. Hennessy and T. A. Betley, *Science*, 2013, **340**, 591–595.
7 Y. Park, Y. Kim and S. Chang, *Chem. Rev.*, 2017, DOI: 10.1021/acs.chemrev.6b00644.
8 (*a*) H. Kim and S. Chang, *ACS Catal.*, 2016, **6**, 2341–2351; (*b*) R. Singh, K. Nagesh and M. Parameshwar, *ACS Catal.*, 2016, **6**, 6520–6524; (*c*) G. Manca, E. Gallo, D. Intrieri and C. Mealli, *ACS Catal.*, 2014, **4**, 823–832.
9 D. A. Iovan and T. A. Betley, *J. Am. Chem. Soc.*, 2016, **138**, 1983–1993.
10 F. Collet, R. H. Dodd and P. Dauban, *Chem. Commun.*, 2009, **34**, 5061–5074.
11 O. Robles and D. Romo, *Nat. Prod. Rep.*, 2014, **31**, 318–334.
12 J. Li, J. S. Cisar, C.-Y. Zhou, B. Vera, H. Williams, A. D. Rodriguez, B. F. Cravatt and D. Romo, *Nat. Chem.*, 2013, **5**, 510–517.
13 (*a*) D. Intrieri, P. Zardi, A. Caselli and E. Gallo, *Chem. Commun.*, 2014, **50**, 11440–11453; (*b*) P. Zardi, A. Caselli, P. Macchi, F. Ferretti and E. Gallo, *Organometallics*, 2014, **33**, 2210–2218.
14 K. Okano, H. Tokuyama and T. Fukuyama, *Chem. Commun.*, 2014, **50**, 13650–13663.
15 K. P. Kornecki and J. F. Berry, *Eur. J. Inorg. Chem.*, 2012, (3), 562–568.
16 I. S. Akhrem, *J. Org. Chem.*, 2015, **793**, 54–77.
17 J. A. McIntosh, P. S. Coelho, C. C. Farwell, Z. J. Wang, J. C. Lewis, T. R. Brown and F. H. Arnold, *Angew. Chem., Int. Ed.*, 2013, **52**, 9309–9312.
18 D. G. Musaev and S. B. Blakey, *Organometallics*, 2012, **31**, 4950–4961.
19 R. Singh, J. N. Kolev, P. A. Sutera and R. Fasan, *ACS Catal.*, 2015, **5**, 1685–1691.
20 R. T. Gephart and T. H. Warren, *Organometallics*, 2012, **31**, 7728–7752.
21 S. M. Paradine, J. R. Griffin, J. Zhao, A. L. Petronico, S. M. Miller and M. C. White, *Nat. Chem.*, 2015, **7**, 987–994.
22 Q. Zhang, C. Wu, L. Zhou and J. Li, *Organometallics*, 2013, **32**, 415–426.
23 Q. Nguyen, T. Nguyen and T. G. Driver, *J. Am. Chem. Soc.*, 2013, **135**, 620–623.
24 H. Wang, Y. Li, Z. Wang, J. Lou, Y. Xiao, G. Qiu, X. Hu, H. J. Altenbach and P. Liu, *RSC Adv.*, 2014, **4**, 25287–25290.
25 G. Manca, C. Mealli, D. M. Carminati, D. Intrieri and E. Gallo, *Eur. J. Inorg. Chem.*, 2015, **29**, 4885–4893.
26 E. T. Hennessy, R. Y. Liu, D. A. Iovan, R. A. Duncan and T. A. Betley, *Chem. Sci.*, 2014, **5**, 1526–1532.
27 (*a*) T. L. Lam, K. C.-H. Tso, B. Cao, C. Yang, D. Chen, X.-Y. Chang, J.-S. Huang and C.-M. Che, *Inorg. Chem.*, 2017, **56**, 4253–4257; (*b*) F. Collet, C. Lescot, C. Liang and P. Dauban, *Dalton Trans.*, 2010, **39**, 10401–10413.
28 A. Nörder, S. A. Warren, E. Herdtweck, S. M. Huber and T. Bach, *J. Am. Chem. Soc.*, 2012, **134**, 13524–13531.
29 J. W. W. Chang, T. M. U. Ton and P. W. H. Chan, *Chem. Rec.*, 2011, **11**, 331–357.
30 C. G. Espino, K. W. Fiori, M. Kim and J. Du Bois, *J. Am. Chem. Soc.*, 2004, **126**, 15378–15379.
31 J. L. Roizen, D. N. Zalatan and J. Du Bois, *Angew. Chem., Int. Ed.*, 2013, **52**, 11343–11346.
32 E. N. Bess, R. J. DeLuca, D. J. Tindall, M. S. Oderinde, J. L. Roizen, J. Du Bois and M. S. Sigman, *J. Am. Chem. Soc.*, 2014, **136**, 5783–5789.
33 K. W. Fiori and J. Du Bois, *J. Am. Chem. Soc.*, 2007, **129**, 562–568.
34 (*a*) R. J. Scamp, J. G. Jirak, N. S. Dolan, I. A. Guzei and J. M. Schomaker, *Org. Lett.*, 2016, **18**, 3014–3017; (*b*) M. E. Harvey, D. G. Musaev and J. Du Bois, *J. Am. Chem. Soc.*, 2011, **133**, 17207–17216; (*c*) J. M. Alderson, A. M. Phelps, R. J. Scamp, N. S. Dolan and J. M. Schomaker, *J. Am. Chem. Soc.*, 2014, **136**, 16720–16723; (*d*) K. W. Fiori, C. G. Espino, B. H. Brodsky and J. Du Bois, *Tetrahedron*, 2009, **65**, 3042–3051.
35 X. H. Zhao, L. W. Chung and Y. D. Wu, *Acc. Chem. Res.*, 2016, **49**, 1302–1310.
36 (*a*) V. Lyaskovskyy, A. I. O. Suarez, H. Lu, H. Jiang, X. P. Zhang and B. de Bruin, *J. Am. Chem. Soc.*, 2011, **133**, 12264–12273; (*b*) Q. Ren, X. Shen, J. Wan and J. Fang, *Organometallics*, 2015, **34**, 1129–1136.
37 (*a*) A. Varela-Álvarez, T. Yang, H. Jennings, K. P. Kornecki, S. N. Macmillan, K. M. Lancaster, J. B. C. Mack, J. Du Bois, J. F. Berry and D. G. Musaev, *J. Am. Chem. Soc.*, 2016, **138**, 2327–2341; (*b*) J. F. Berry, *Dalton Trans.*, 2012, **41**, 700–713; (*c*) X. Zhang, H. Xu and C. Zhao, *J. Org. Chem.*, 2014, **79**, 9799–9811; (*d*) H. Xu, X. Zhang, Z.-F. Ke, Z.-F. Li, X.-Y. Xu, C.-Y. Su, D. L. Phillips and C. Zhao, *RSC Adv.*, 2013, **3**, 17131–17142; (*e*) H. Xu, K. Muto, J. Yamaguchi, C. Zhao, K. Itami and D. G. Musaev, *J. Am. Chem. Soc.*, 2014, **136**, 14834–14844.
38 (*a*) J. Wang, C. Zhao, Y. Weng and H. Xu, *Catal. Sci. Technol.*, 2016, **6**, 5292–5303; (*b*) J. Wang, Theore-tical Studies on the Mechanisms of C-N/C Formation and Cleavage Promoted by Transition Metal Complexes, Ph.D. thesis, Sun Yat-sen University, 2010.
39 J. Wang, H. Xu, H. Gao, C.-Y. Su, C. Zhao and D. L. Phillips, *Organometallics*, 2010, **29**, 42–51.
40 (*a*) J. Wang, K. Zheng, T.-F. Miao and E. Zhang, *Sci. Adv. Mater.*, 2017, **9**, 1197–1208; (*b*) K. Zheng, J. Wang, Y. Shen, W. Peng and F. Yun, *J. Comput. Chem.*, 2002, **23**, 436–443; (*c*) K. Zheng, J. Wang, Y. Shen, W. Peng and F. Yun, *Dalton Trans.*, 2002, (1), 111–116; (*d*) K. Zheng, J. Wang, Y. Shen, D. Kuang and F. Yun, *J. Phys. Chem. A*, 2001, **105**, 7248–7253.
41 M. J. Frisch, G. W. Trucks, H. B. Schlegel, G. E. Scuseria, M. A. Robb, J. R. Cheeseman, G. Scalmani, V. Barone, B. Mennucci, G. A. Petersson, H. Nakatsuji, M. Caricato,

Open Access Article. Published on 11 July 2017. Downloaded on 2/7/2026 5:24:19 AM.
This article is licensed under a Creative Commons Attribution-NonCommercial 3.0 Unported Licence.

X. Li, H. P. Hratchian, A. F. Izmaylov, J. Bloino, G. Zheng, J. L. Sonnenberg, M. Hada, M. Ehara, K. Toyota, R. Fukuda, J. Hasegawa, M. Ishida, T. Nakajima, Y. Honda, O. Kitao, H. Nakai, T. Vreven, J. A. Montgomery Jr, J. E. Peralta, F. Ogliaro, M. Bearpark, J. J. Heyd, E. Brothers, K. N. Kudin, V. N. Staroverov, T. Keith, R. Kobayashi, J. Normand, K. Raghavachari, A. Rendell, J. C. Burant, S. S. Iyengar, J. Tomasi, M. Cossi, N. Rega, J. M. Millam, M. Klene, J. E. Knox, J. B. Cross, V. Bakken, C. Adamo, J. Jaramillo, R. Gomperts, R. E. Stratmann, O. Yazyev, A. J. Austin, R. Cammi, C. Pomelli, J. W. Ochterski, R. L. Martin, K. Morokuma, V. G. Zakrzewski, G. A. Voth, P. Salvador, J. J. Dannenberg, S. Dapprich, A. D. Daniels, O. Farkas, J. B. Foresman, J. V. Ortiz, J. Cioslowski, and D. J. Fox, *Gaussian 09, Revision D.01*, Gaussian, Inc., Wallingford CT, 2013.

42 Y. Zhao and D. G. Truhlar, *J. Chem. Phys.*, 2006, **125**, 194101.

43 S. J. Gustafson, J. T. Fuller III, D. Devarajan, J. Snyder, R. A. Periana, B. G. Hashiguchi, M. M. Konnick and D. H. Ess, *Organometallics*, 2015, **34**, 5485–5495.

44 T. Sperger, I. A. Sanhueza, I. Kalvet and F. Schoenebeck, *Chem. Rev.*, 2015, **115**, 9532–9586.

45 T. G. Driver, *Nat. Chem.*, 2013, **5**, 736–738.

46 (*a*) U. Steinbrenner, A. Bergner, M. Dolg and H. Stoll, *Mol. Phys.*, 1994, **82**, 3–11; (*b*) A. Henglein, *J. Phys. Chem.*, 1993, **97**, 5457–5471; (*c*) M. Kaupp, P. V. R. Schleyer, H. Stoll and H. Preuss, *J. Chem. Phys.*, 1991, **94**, 1360–1366; (*d*) W. H. Lam, K. C. Lam, Z. Lin, S. Shimada, R. N. Perutz and T. B. Marder, *Dalton Trans.*, 2004, (10), 1556–1562.

47 (*a*) W. J. Hehre, R. Ditchfield and J. A. Pople, *J. Chem. Phys.*, 1972, **56**, 2257; (*b*) J. D. Dill and J. A. Pople, *J. Chem. Phys.*, 1975, **62**, 2921.

48 P. C. Hariharan and J. A. Pople, *Mol. Phys.*, 1974, **27**, 209–214.

49 (*a*) K. J. Fukui, *J. Phys. Chem.*, 1970, **74**, 4161–4163; (*b*) K. Fukui, *Acc. Chem. Res.*, 1981, **14**, 363–368.

50 (*a*) R. Krishnan, J. S. Binkley, R. Seeger and J. A. Pople, *J. Chem. Phys.*, 1980, **72**, 650–654; (*b*) R. Ditchfield, W. J. Hehre and J. A. Pople, *J. Chem. Phys.*, 1971, **54**, 724.

51 A. V. Marenich, C. J. Cramer and D. G. Truhlar, *J. Phys. Chem. B*, 2009, **113**, 6378–6396.

52 E. D. Glendening, J. K. Badenhoop, A. E. Reed, J. E. Carpenter and J. A. Bohmann, C. M. Morales, C. R. Landis and F. Weinhold, *NBO 6.0*, Theoretical Chemistry Institute, University of Wisconsin, Madison, 2013.

53 C. Kong, N. Jana, C. Jones and T. G. Driver, *J. Am. Chem. Soc.*, 2016, **138**, 13271–13280.

54 N. Dolan, R. J. Scamp, T. Yang, J. F. Berry and J. M. Schomaker, *J. Am. Chem. Soc.*, 2016, **138**, 14658–14667.

55 J. G. Harrison, O. Gutierrez, N. Jana, T. G. Driver and D. J. Tantillo, *J. Am. Chem. Soc.*, 2016, **138**, 487–490.

56 B. Bagh, D. L. J. Broere, V. Sinha, P. F. Kuijpers, N. P. V. Leest, B. D. Bruin, S. Demeshko, M. A. Siegler and J. I. V. D. Vlugt, *J. Am. Chem. Soc.*, 2017, **139**, 5117–5124.

This journal is © The Royal Society of Chemistry 2017